Bone Reports 18 (2023) 101662

Contents lists available at ScienceDirect

Bone Reports

journal homepage: www.elsevier.com/locate/bonr

C3a-C3aR signaling is a novel modulator of skeletal homeostasis

Megan B. Kuhn [a], Hayden S. VandenBerg [a], Andrew J. Reynolds [a], Matthew D. Carson [a,b,c], Amy J. Warner [a,b,c], Amanda C. LaRue [d,e,f], Chad M. Novince [a,b,c], Jessica D. Hathaway-Schrader [b,d,e,*]

[a] Department of Oral Health Sciences, College of Dental Medicine, Medical University of South Carolina, Charleston, SC, USA
[b] Department of Stomatology-Div. of Periodontics, College of Dental Medicine, Medical University of South Carolina, Charleston, SC, USA
[c] Department of Pediatrics-Div. of Endocrinology, College of Medicine, Medical University of South Carolina, Charleston, SC, USA
[d] Research Services, Ralph H. Johnson Department of Veterans Affairs Health Care System, Charleston, SC, USA
[e] Department of Pathology and Laboratory Medicine, College of Medicine, Medical University of South Carolina, Charleston, SC, USA
[f] Hollings Cancer Center, Medical University of South Carolina, Charleston, SC, USA

ARTICLE INFO

Keywords:
Osteoimmunology
Complement
Osteoblast
Osteoclast

ABSTRACT

Osteoimmune studies have identified complement signaling as an important regulator of the skeleton. Specifically, complement anaphylatoxin receptors (i.e., C3aR, C5aR) are expressed on osteoblasts and osteoclasts, implying that C3a and/or C5a may be candidate mediators of skeletal homeostasis. The study aimed to determine how complement signaling influences bone modeling/remodeling in the young skeleton. Female C57BL/6J $C3aR^{-/-}C5aR^{-/-}$ vs. wildtype and $C3aR^{-/-}$ vs. wildtype mice were examined at age 10 weeks. Trabecular and cortical bone parameters were analyzed by micro-CT. In situ osteoblast and osteoclast outcomes were determined by histomorphometry. Osteoblast and osteoclast precursors were assessed in vitro. $C3aR^{-/-}C5aR^{-/-}$ mice displayed an increased trabecular bone phenotype at age 10 weeks. In vitro studies revealed $C3aR^{-/-}C5aR^{-/-}$ vs. wildtype cultures had less bone-resorbing osteoclasts and increased bone-forming osteoblasts, which were validated in vivo. To determine whether C3aR alone was critical for the enhanced skeletal outcomes, wildtype vs. $C3aR^{-/-}$ mice were evaluated for osseous tissue outcomes. Paralleling skeletal findings in $C3aR^{-/-}C5aR^{-/-}$ mice, $C3aR^{-/-}$ vs. wildtype mice had an enhanced trabecular bone volume fraction, which was attributed to increased trabecular number. There was elevated osteoblast activity and suppressed osteoclastic cells in $C3aR^{-/-}$ vs. wildtype mice. Furthermore, primary osteoblasts derived from wildtype mice were stimulated with exogenous C3a, which more profoundly upregulated *C3ar1* and the pro-osteoclastic chemokine *Cxcl1*. This study introduces the C3a/C3aR signaling axis as a novel regulator of the young skeleton.

1. Introduction

The field of osteoimmunology has demonstrated that innate and adaptive immune interactions with bone cells modulate skeletal development and maturation (Li et al., 2007a; Lorenzo et al., 2008; Takayanagi, 2009; Walsh et al., 2018). Proinflammatory immune signaling augments osteoclastogenesis while suppressing osteoblastic bone formation. Thus, this proinflammatory milieu can have unfavorable effects on maintaining skeletal homeostasis (Redlich and Smolen, 2012; Zaidi, 2007; Weitzmann and Ofotokun, 2016). The human skeleton accumulates peak bone mass during the pubertal/post-pubertal growth window up until around 30 years of age, and thereafter begins a process of slow continuous bone loss throughout life (Baxter-Jones et al., 2011; Weaver et al., 2016). Appreciating that approximately 40 % of peak bone accrual occurs during the pubertal/post-pubertal phase (Bonjour et al., 1991; Cheung et al., 2011; McCormack et al., 2017), there is a critical need to improve our understanding of osteoimmunological processes regulating the attainment of bone mass during this period.

Previous osteoimmunology studies revealed that innate immune complement signaling may be critical in bone cell actions (Sato et al., 1993; Tu et al., 2010; Ignatius et al., 2011; Pobanz et al., 2000; Matsuoka et al., 2014; Kovtun et al., 2017; Modinger et al., 2018). The complement cascade comprises a network of interacting molecules that initiate, promote, and modulate immune and inflammatory responses (Ricklin et al., 2010). The components of the complement cascade work together to direct a host response to tissue injury or infection (Ricklin

* Corresponding author at: 30 Courtenay Drive, Research Services, Ralph H. Johnson VAHCS, Charleston, SC 29425, USA.
E-mail address: hathawa@musc.edu (J.D. Hathaway-Schrader).

https://doi.org/10.1016/j.bonr.2023.101662
Received 10 September 2022; Received in revised form 13 February 2023; Accepted 15 February 2023
Available online 16 February 2023

et al., 2010). Complement signaling is also responsible for inflammatory interactions with toll-like receptors (TLRs) and regulating the activation, differentiation, and maintenance of B-cells and T-cell subsets (Hajishengallis and Lambris, 2016). While complement can be initiated by either the classical, lectin or alternative pathways, all pathways converge at C3 cleavage for downstream molecules to modulate several functions. C3 and C5 are cleaved by convertases and generate the anaphylatoxins C3a and C5a, which regulate crosstalk with TLRs and inflammatory cell recruitment and activation (Hajishengallis and Lambris, 2016; Reis et al., 2019). C3a and C5a induce inflammatory actions through signaling at their cognate receptors C3aR and C5aR. These receptors are expressed on cells of both hematopoietic and mesenchymal stem cell origins (Reis et al., 2019).

Complement signaling may play a critical role in osteoblast and osteoclast differentiation and function (Sato et al., 1993; Tu et al., 2010; Ignatius et al., 2011; Pobanz et al., 2000; Matsuoka et al., 2014; Kovtun et al., 2017; Modinger et al., 2018). It has been demonstrated that C3 expression can induce bone marrow stromal cell (BMSC) secretion of proinflammatory cytokines while exogenous C3aR agonists can stimulate in vitro osteoclast differentiation (Sato et al., 1993; Tu et al., 2010) and mediate osteoblast-osteoclast coupling (Matsuoka et al., 2014). Reports have shown that C3aR and C5aR can be expressed on osteoblasts and osteoclasts (Sato et al., 1993; Tu et al., 2010; Ignatius et al., 2011). While global $C3^{-/-}$ and $C5^{-/-}$ mice displayed no differences in bone volume fraction at age 12 weeks (Ehrnthaller et al., 2013), C5aR1 null mice have increased bone mass accrual (Kovtun et al., 2017). Thus, prior osteoimmunology studies have focused on C5aR in fracture healing of the adult skeleton (Kovtun et al., 2017; Ehrnthaller et al., 2013; Recknagel et al., 2012; Ehrnthaller et al., 2016; Bergdolt et al., 2017). However, the role of C3a/C3aR signaling in the growing skeleton is currently unknown.

In C57BL/6J mice, the pubertal/post pubertal developmental phase has been estimated to begin around age 6 weeks, bone modeling (growth) is considered principally complete at age 12 weeks, and bone mineral density peaks around age 18 weeks (Landreth, 2002; Ferguson et al., 2003; Glatt et al., 2007). The current report investigates C3aR/C5aR and C3aR signaling in C57BL/6J mice during post pubertal skeletal growth. Outcomes from this study reveal that C3a/C3aR signaling has pro-osteoclastic/anti-osteoblastic actions on the skeleton, providing initial evidence that complement signaling factors influence osteoimmune crosstalk to regulate skeletal growth.

2. Materials and methods

2.1. Mice

Female wildtype C57BL/6 mice were purchased from Jackson Laboratories and housed in ventilated cages in a specific-pathogen-free vivarium. Female $C3aR^{-/-}C5aR^{-/-}$ and $C3aR^{-/-}$ mice were gifted by Dr. Carl Atkinson (University of Florida). Mice were euthanized at 10 weeks of age. Room temperature and humidity were carried out within recommended ranges of the Guide for the Care and Use of Laboratory Animals (8th Ed.). All work with mice was approved by the MUSC Animal Protocols Review Board, performed in accordance with the National Institute of Health Guide for Care and Use of Laboratory Animals, and reported by the ARRIVE guidelines.

2.2. Micro-CT

Femurs were harvested and fixed in 10 % neutral-buffered-formalin. Specimens were scanned with Scanco micro-CT 40 Scanner (Scanco Medical): X-ray tube potential = 70 kVp; Integration time = 200 ms; voxel size = 10 μm^3. Calibrated three-dimensional images were reconstructed. The software Analyze 12.0 Bone Microarchitecture Analysis (AnalyzeDirect) was utilized for trabecular bone at the distal femur and cortical bone at the femoral mid-diaphysis. Trabecular bone was evaluated in axial CT sections starting at 300 μm proximal to the distal growth plate and extending 1000 μm proximally. Cortical bone was assessed in transverse CT slices in a 1000um segment of the mid-diaphysis. A fixed threshold of 1750 Hounsfield units discerned mineralized tissue. Data are reported following standardized nomenclature (Bouxsein et al., 2010).

2.3. In situ immunofluorescence

Tibiae were fixed in 10 % phosphate-buffered-formalin for 24 h at room temperature. Long bones were decalcified in 14 % EDTA for 21 days at room temperature, paraffin-embedded, and samples were cut into 5 μm serial frontal sections. Specimens were deparaffinized, rehydrated, and incubated in 0.2 M boric acid at 60 °C overnight for antigen retrieval. Specimens were then incubated with a 1:100 dilution of anti-osterix (OSX) monoclonal antibody (Santa Cruz Biotechnology) for 2 h at room temperature. Sections were washed in 1× PBS and then incubated with a 1:2000 FITC-goat anti-rabbit (Santa Cruz Biotechnology) for 1 h at room temperature (protected from light). Samples were washed with 1× PBS and mounted via ProLong Diamond Antifade Mountant with DAPI (Life Technologies). OSX+ osteoblastic cells lining bone were evaluated in the proximal tibia. The region of interest for analysis was the secondary spongiosa, initiated 250 μm distal to the proximal growth plate and extending 1000 μm distally; 50 μm from endocortical surfaces. Images were acquired at 100× utilizing the Keyence BZ-19 X810 microscope (Keyence) and scored via ImageJ software.

2.4. Histomorphometry

Tibiae were collected and fixed in 10 % neutral-buffered formalin, decalcified in 14 % EDTA, and processed for paraffin histology. Five-μm serial frontal sections were acquired of the proximal tibia. Tibia sections were stained with tartrate-resistant acid phosphatase (TRAP) and counterstained with hematoxylin for histomorphometric analyses of osteoclasts. TRAP+ multinucleated (≥3 nuclei) cells lining trabecular bone were scored as osteoclasts. The region of interest for analysis in proximal tibiae sections was carried out as previously described (Hathaway-Schrader et al., 2019; Hathaway-Schrader et al., 2020). Images were acquired at 200× using a Keyence BZ-X810 microscope and analyzed using ImageJ software. Data are reported following standardized nomenclature (Dempster et al., 2013), as previously described (Hathaway-Schrader et al., 2019, 2020).

2.5. Bone marrow cultures

For each animal, femurs and tibiae were flushed for bone marrow using α-MEM media (Gibco, Fisher Scientific) supplemented with 20 % FBS (Hyclone) and 1 % PSG (2 mM glutamine, 100 U/mL penicillin, 100 mg/mL streptomycin). Cells were disassociated and plated in a 60 mm dish. Twenty-four hours after plating, hematopoietic progenitor cell fraction was isolated for osteoclast-precursor (OCP) assays by decanting off the non-adherent cells. Fresh α-MEM media supplemented with 20 % FBS (Hyclone) and 1 % PSG was added back to the bone marrow cultures; 48 h later, adherent cells were isolated for bone marrow stromal cell (BMSC) assays. Cultures were not combined from animals for initial bone marrow cultures or subsequent OCP/BMSC assays; n-values reported for in vitro assays represent biological replicates.

2.6. In vitro bone marrow stromal cell (BMSC) assays

Adherent BMSCs were isolated from bone marrow cultures. BMSCs were washed, counted, and plated for assays in α-MEM media, 10 % FBS (Hyclone), and 1 % PSG. Cell expansion assay: BMSCs were plated at 2.0 × 10^4 cells/cm^2 in 48-well plates in α-MEM media, 10 % FBS (Hyclone), and 1 % PSG. Cells were collected on day 2, day 4, day 6, day 8, and day 10 for cell counts (Novince et al., 2017). Von Kossa osteogenesis assay:

BMSCs were plated at 1.0×10^5 cells/cm^2 in 48-well plates with α-MEM media supplemented with 10 % FBS (Hyclone) and 1 % PSG for 3 days. Confluent cultures were then treated with osteogenic media (α-MEM media, 10 % FBS (Hyclone), 1 % PSG, 50 mg/mL ascorbic acid, and 10 mM β-glycerophosphate) for 11 days. Cultures were stained by the von Kossa method to detect mineralization, as previously reported (Hathaway-Schrader et al., 2020, 2022). Differentiation potential quantitative real-time PCR (qRT-PCR) assay: BMSCs were plated at 2.0×10^4 cells/cm^2 in 12-well plates and cultured in α-MEM media, 10 % FBS, 1 % PSG, to assess alterations in multipotent differentiation potential in unstimulated cultures. Day-4 pre-confluent cultures were collected for qRT-PCR gene expression analysis to evaluate alterations in BMSC commitment towards the osteoblastogenic, adipogenic, and chondrogenic lineages (Hathaway-Schrader et al., 2019, 2020; Novince et al., 2017). Unstimulated BMSC RNA was isolated by the TRIzol Reagent (Invitrogen) method. Total RNA was quantified via NanoDrop 1000 (Thermo Fisher Scientific). cDNA was generated using TaqMan Random Hexamers and Reverse Transcription Reagents (Applied Biosystems) and amplified by TaqMan primers and Universal PCR Master Mix by the StepOnePlus System (Applied Biosystems). *Gapdh* was used as an internal control gene; relative quantification of data was carried out by the comparative C_T method ($2^{-\Delta\Delta CT}$) (Schmittgen and Livak, 2008), as previously described (Hathaway-Schrader et al., 2019; Novince et al., 2017). Osteogenic potential qRT-PCR assay: BMSCs were plated at 2.0×10^4 cells/cm^2 in 12-well plates and cultured in α-MEM media, 10 % FBS, 1 % PSG until reaching confluency. Confluent cultures were then treated with α-MEM media supplemented with 10 % FBS, 1 % PSG, and 50 mg/mL ascorbic acid for 5 days, as previously described (Hathaway-Schrader et al., 2020; Novince et al., 2017). Cultures were then collected for qRT-PCR analysis of *Bglap (Ocn)* mRNA, as stated previously.

2.7. In vitro osteoclast-precursor assays

Non-adherent hematopoietic progenitor cells separated from bone marrow cultures were washed and incubated with CD11b microbeads (Miltenyi Biotec, Bergisch Gladbach, Germany). AutoMACS Sorter (Miltenyi Biotec) was employed to separate CD11b$^-$ hematopoietic progenitor cells, as previously described (Hathaway-Schrader et al., 2019; Novince et al., 2017). TRAP stain assay: The CD11b$^-$ cellular fraction was plated at 1.5×10^5 cells/cm^2 in 96-well plates in α-MEM media, 10 % FBS (Hyclone), 1 % PSG. Cells were primed for 36 h with 10 ng/mL CSF1 (R&D Systems, Minneapolis, MN, USA) to enhance CD11b$^-$ OCP cells, which have high osteoclastic potential (Jacquin et al., 2006). CD11b$^-$ OCP cultures were then stimulated with either fresh control (25 ng/mL CSF1) or treatment (25 ng/mL CSF1 + 50 ng/mL RANKL; R&D Systems) media for 5 days; media was refreshed every other day. Control and treatment cultures were stained by the TRAP method, as previously reported (Hathaway-Schrader et al., 2020; Novince et al., 2017). TRAP-stained cultures were carried out in triplicate wells for each animal (biological replicate). Entire culture wells were imaged at 200× using the Keyence BZ-X810 microscope (Keyence, Osaka, Japan). TRAP+ cells with three or greater nuclei were scored as osteoclasts for cytomorphometric analyses. Osteoclast cellular outcomes included number of osteoclasts per well (N.Oc/Well), average osteoclast area (Oc.Ar/Oc), and nuclei number per osteoclast (N.Nc/Oc). Analysis was performed using NIH ImageJ software, version 1.51j8, https://imagej.nih.gov/ij/ (NIH, Bethesda, MD). Gene expression assay: CD11b$^-$ cellular fraction was plated in 12-well plates in α-MEM media, 10 % FBS (Hyclone), 1 % PSG and primed for 36 h with 10 ng/mL CSF1. CD11b$^-$ OCP cultures were then stimulated with either fresh control (25 ng/mL CSF1) or treatment (25 ng/mL CSF1 and 50 ng/mL RANKL) media for 4 days. Media was changed every 2 days. Day-4 control cultures (25 ng/mL CSF1) and treatment cultures (25 ng/mL CSF1 and 50 ng/mL RANKL) were isolated for quantitative real-time PCR (qRT-PCR) mRNA analysis. Gene expression assay was carried out in duplicate (technical replicate) cultures.

2.8. In vitro C3a-osteoblast stimulation assay

BMSCs were plated in culture media (α-MEM media + 10 % Hyclone FBS + 1 % PSG) at 2.0×10^4 cells/cm^2 in 12-well plates. Upon reaching confluency, cultures were stimulated with osteogenic media (α-MEM media + 10 % Hyclone FBS + 1 % PSG + 50μg/mL ascorbic acid) for 5 days, media changed every other day. Cells were then cultured overnight in serum-deprived osteogenic media (α-MEM media +0.3 % Hyclone FBS + 1 % PSG + 50μg/mL ascorbic acid). On Day-6, cultures were stimulated for 2 h with serum-deprived osteogenic media supplemented with either vehicle-control or recombinant C3a (5, 10, or 20 ng/mL, R&D Systems). After the 2-h stimulation, supernatants were aspirated, and cells were washed to remove recombinant proteins. Fresh serum-deprived osteogenic media was added back to cultures for 5 h. Cell culture supernatants were then collected for ELISA protein assays, and cells were isolated for qRT-PCR gene expression analysis to assess pro-osteoclastic genes. In vitro osteoblast stimulation assay was performed in triplicate (technical replicate) cultures. Data are representative of two separate experiments.

2.9. Serum biochemical assay

Whole blood was collected via cardiac puncture at euthanasia, serum was isolated, and stored at -80 °C. P1NP (Immunodiagnostic Systems, East Boldon, UK) was tested by ELISA, per the manufacturer's procedures. Supernatants were collected from vehicle-control and C3a-stimulated osteoblast cultures and stored at -80 °C. C3 (Abcam, Cambridge, UK) was assessed by ELISA, following the manufacturer's protocols.

2.10. Statistics

Unpaired two-tailed *t*-tests compared wildtype vs. C3aR$^{-/-}$C5aR$^{-/-}$ and wildtype vs. C3aR$^{-/-}$; GraphPad Prism 8.7 (GraphPad Software Inc.). For in vitro osteoblast C3a stimulation assays, one-way ANOVA was carried out in C3a dose response cultures. Data are reported as mean ± SEM.

3. Results

3.1. Knockdown of complement C3aR and C5aR enhances bone morphology

Micro-CT analysis was executed in the femur of C3aR$^{-/-}$C5aR$^{-/-}$ vs. wildtype mice to investigate tissue level alterations in cancellous (Fig. 1A-G) and cortical (Fig. 1H-K) bone. C3aR$^{-/-}$C5aR$^{-/-}$ vs. wildtype mice had elevated trabecular bone mineral density (Fig. 1B) and a 20.8 % increase in bone volume fraction (Fig. 1C). Trabecular microarchitecture outcomes in C3aR$^{-/-}$C5aR$^{-/-}$ mice showed higher connectivity density (Fig. 1D), increased trabecular number (Fig. 1E), and reduced trabecular separation (Fig. 1G). Cortical bone mineral density (Fig. 1I) was increased while cortical thickness (Fig. 1K) was similar in the femoral mid-diaphysis of C3aR$^{-/-}$C5aR$^{-/-}$ vs. wildtype mice. These outcomes support that C3aR/C5aR signaling adversely affects bone mass accrual and microarchitecture during post-pubertal skeletal maturation.

3.2. Elevated osteoblastogenesis in C3aR$^{-/-}$C5aR$^{-/-}$ vs. wildtype mice

C3aR and C5aR are expressed on osteoblasts (Sato et al., 1993; Tu et al., 2010; Ignatius et al., 2011). In vitro experiments were carried out in BMSCs derived from C3aR$^{-/-}$C5aR$^{-/-}$ vs. wildtype mice to determine the role of C3aR and C5aR in osteoblastogenesis (Fig. 2). Unstimulated BMSC expansion was enhanced in C3aR$^{-/-}$C5aR$^{-/-}$ vs. wildtype cultures over time (Fig. 2A). Gene expression was evaluated in pre-confluent untreated day-4 BMSC cultures for alterations in mesenchymal-stromal cell differentiation potential (Fig. 2B). Untreated day-4 BMSC cultures

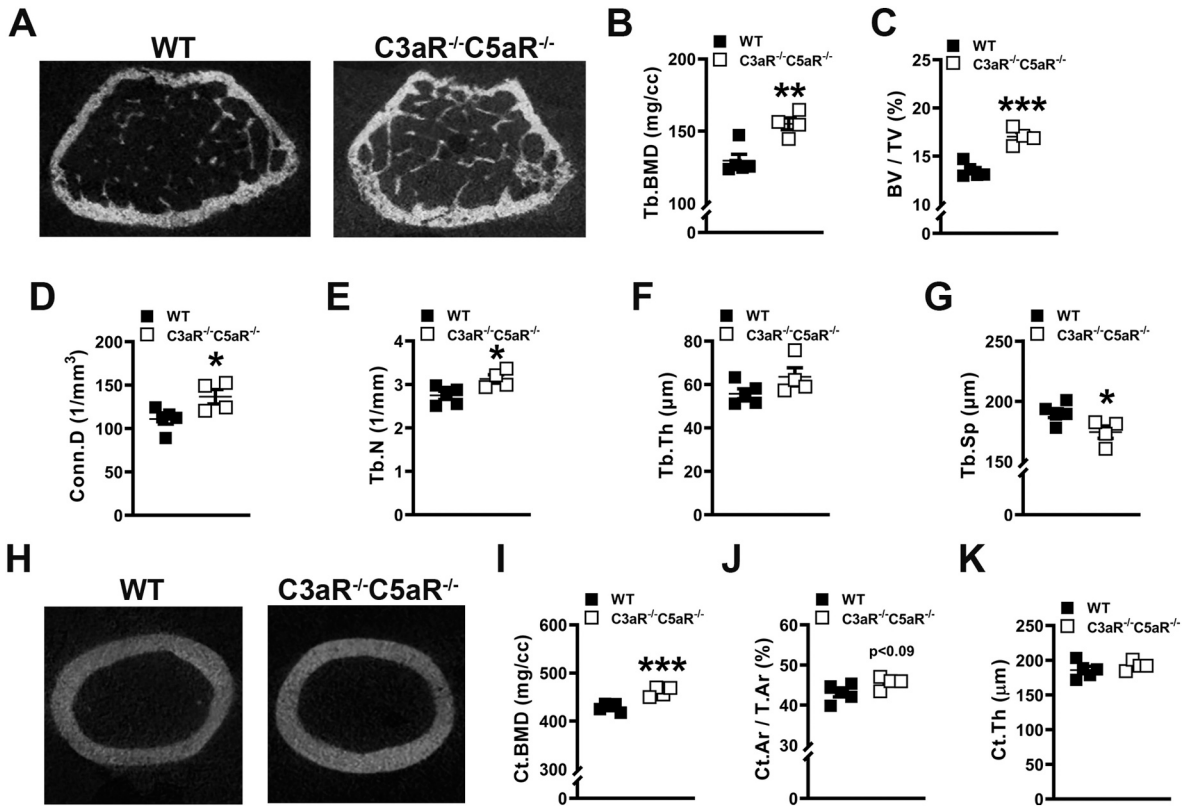

Fig. 1. Knockdown of complement C3aR and C5aR enhances bone morphology. Wildtype (WT) and C3aR$^{-/-}$C5aR$^{-/-}$ mice were euthanized, and femurs were analyzed. (A-G) WT vs. C3aR$^{-/-}$C5aR$^{-/-}$ micro-CT trabecular analysis, (n = 4–5 mice/group). A. Representative micro-CT images of trabecular bone at the distal femur. B. Trabecular (Tb) bone mineral density (BMD). C. Trabecular bone volume fraction (BV/TV). D. Connectivity density (Conn.D). E. Trabecular number (Tb.N). F. Trabecular thickness (Tb.Th). G. Trabecular Separation (Tb.Sp). (H-K) WT vs. C3aR$^{-/-}$C5aR$^{-/-}$ micro-CT cortical analysis, (n = 4–5 mice/group). H. Representative micro-CT images of femur mid-diaphysis. I. Cortical BMD. J. Cortical bone area fraction (Ct.Ar/T.Ar). K. Cortical thickness (Ct.Th). Data are expressed as mean ± SEM, *$p < 0.05$, **$p < 0.01$, ***$p < 0.001$.

showed no difference in the commitment to the adipogenic (*Pparg*) or chondrogenic (*Col2a1*) lineages and increased commitment to the osteogenic (*Sp7*) lineage (Fig. 2B). Because of the elevated osteogenic potential in unstimulated BMSCs, C3aR$^{-/-}$C5aR$^{-/-}$ vs. wildtype cultures were treated with ascorbic acid for 5 days and collected for qRT-PCR analysis. *Bglap (Ocn)* was upregulated in C3aR$^{-/-}$C5aR$^{-/-}$ vs. wildtype cultures (Fig. 2C). Supporting the gene expression results from stimulated cells, von Kossa assays demonstrated increased mineralization potential in BMSC cultures from C3aR$^{-/-}$C5aR$^{-/-}$ vs. wildtype mice (Fig. 2D). These data suggest that C3aR/C5aR signaling in osteoblastic cells suppresses osteogenesis.

To validate in vitro osteoblastogenesis findings, in situ immunofluorescent staining and histomorphometric analysis of proximal tibia sections was carried out to evaluate OSX+ bone-lining osteoblasts in wild-type vs. C3aR$^{-/-}$C5aR$^{-/-}$ mice (Fig. 2E-F). The frequency of OSX+ osteoblasts was increased (Fig. 2F), while serum P1NP levels were enhanced in C3aR$^{-/-}$C5aR$^{-/-}$ vs. wildtype mice (Fig. 2G). This data supports the notion that complement receptors C3aR and C5aR alter osteoblastogenesis in growing mice.

3.3. Suppressed osteoclastogenesis in C3aR$^{-/-}$C5aR$^{-/-}$ vs. wildtype mice

Cytomorphometric analysis of day-5 osteoclast-precursor (OCP) cell cultures from C3aR$^{-/-}$C5aR$^{-/-}$ vs. wildtype mice (Fig. 3A-D) revealed blunted osteoclastogenic differentiation potential in C3aR$^{-/-}$C5aR$^{-/-}$ OCPs. The number of osteoclasts (N.Oc/Well; Fig. 3B) and numbers of nuclei per osteoclast (N.Nc/Oc; Fig. 3D) were decreased in OCP cultures from C3aR$^{-/-}$C5aR$^{-/-}$ vs. wildtype mice. These data demonstrate that C3aR/C5aR signaling in OCP cells promotes osteoclastogenesis. To confirm cytomorphometric findings, *Dcstamp*, a RANKL-induced transmembrane protein critical for osteoclast fusion, was examined in Day-4 CD11b^{-} OCP treatment vs. control cultures (Fig. 3E). RANKL treatment more profoundly upregulated *Dcstamp* in CD11b^{-} OCP cultures from wild-type vs. C3aR$^{-/-}$C5aR$^{-/-}$ mice (Fig. 3E). This suggests that the C3aR/C5aR immunostimulation promotes RANKL-induced osteoclast fusion.

Histomorphometric analysis of TRAP-stained proximal tibia sections was performed to determine if osteoclastogenesis was decreased in the absence of C3aR/C5aR in vivo (Fig. 3F-I). There was no change in the number of osteoclasts lining the trabecular bone perimeter (N.Oc/B.Pm) in C3aR$^{-/-}$C5aR$^{-/-}$ vs. wildtype mice (Fig. 3G). Osteoclast size (Oc.Ar/Oc; Fig. 3H) was smaller and the osteoclast perimeter per bone perimeter (Oc.Pm/B.Pm; Fig. 3I) was reduced in C3aR$^{-/-}$C5aR$^{-/-}$ vs. wildtype mice, which suggests that C3aR/C5aR signaling supports osteoclast maturation. The decreased Oc.Ar/Oc (Fig. 3H) and Oc.Pm/B.Pm (Fig. 3I) findings in the proximal tibia of C3aR$^{-/-}$C5aR$^{-/-}$ vs. wildtype mice were consistent with the enhanced osteoclast numbers (Fig. 3B) and maturation potential (Fig. 3D) found in the Day-5 OCP culture system. The suppressed osteoclastic phenotype and superior trabecular bone phenotype (Fig. 1) observed in C3aR$^{-/-}$C5aR$^{-/-}$ vs. wildtype mice supports that C3aR/C5aR signaling has catabolic effects on trabecular bone.

3.4. C3aR$^{-/-}$ vs. wildtype mice have a superior trabecular bone phenotype

Our studies in C3aR$^{-/-}$C5aR$^{-/-}$ vs. wildtype mice demonstrated that C3aR/C5aR signaling impairs bone quantity and quality in the post

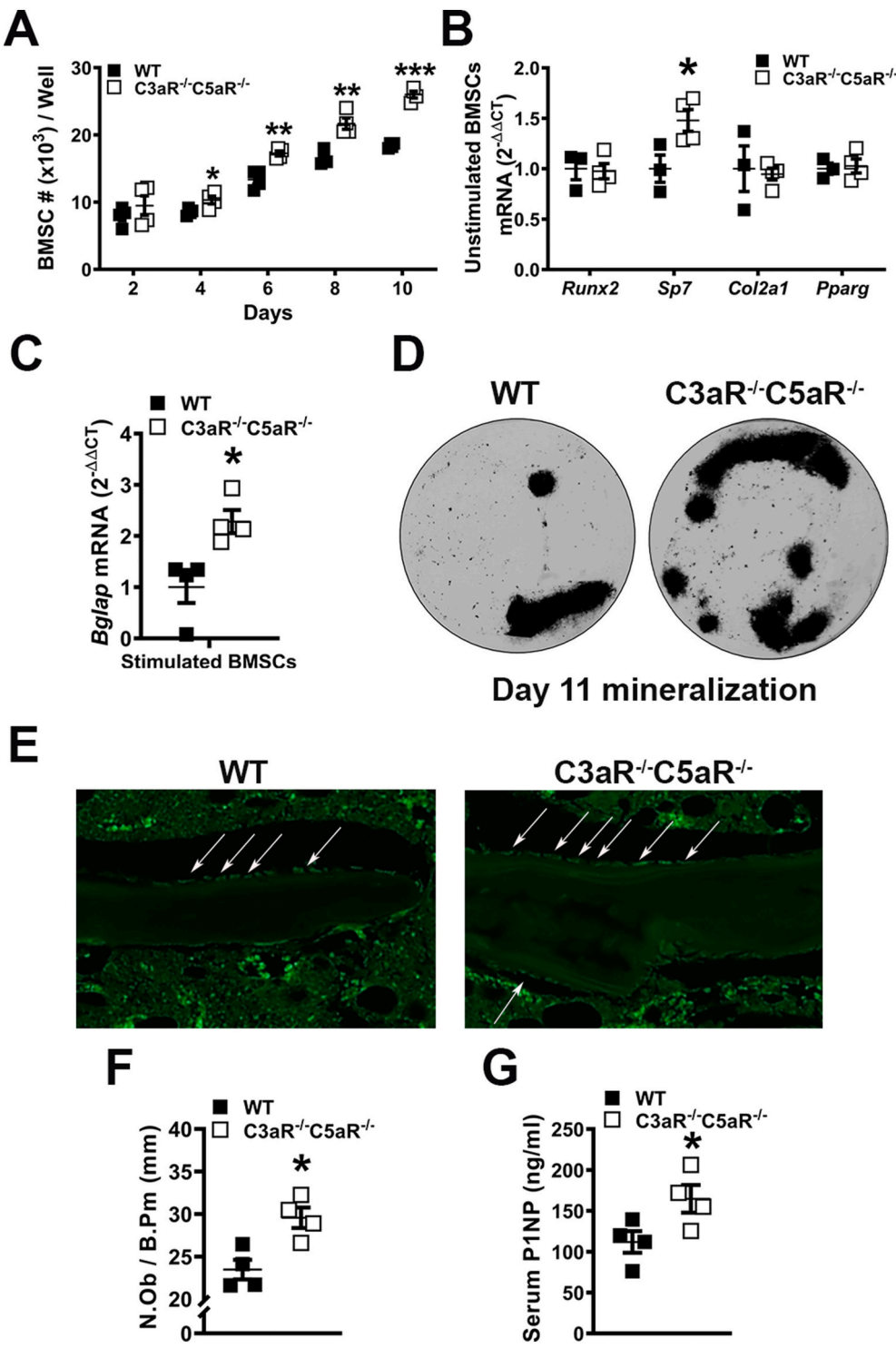

Fig. 2. Elevated osteoblast differentiation and function in C3aR$^{-/-}$C5aR$^{-/-}$ vs. wildtype cultures. (A–D) Wildtype (WT) and C3aR$^{-/-}$C5aR$^{-/-}$ mice were euthanized, bone marrow harvested, and BMSCs were isolated for in vitro assays. A. BMSC expansion over time in culture. B. BMSC differentiation potential assay; BMSCs were cultured for 4 days and harvested pre-confluent for qRT-PCR analysis. mRNA markers for osteoblastic (*Runx2*, *Sp7*), chondrogenic (*Col2a1*), and adipogenic (*Pparg*) potential were evaluated, and relative quantification of mRNA was performed via the comparative *CT* method ($2^{-\Delta\Delta CT}$). C. BMSC osteogenic potential assay: BMSCs stimulated with osteogenic media for 5 days were isolated for qRT-PCR analysis of *Bglap (Ocn)* mRNA. D. Representative images of day 11 mineralization cultures stained by the von Kossa method. Cultures (n = 3–4 mice/group) were carried out in duplicate. (*E*-F) WT and C3aR$^{-/-}$C5aR$^{-/-}$ mice were euthanized, and tibiae were processed for paraffin-embedded in situ immunofluorescent staining for osterix (OSX+) bone-lining osteoblasts (n = 4 mice/group). E. Representative images of OSX-stained proximal tibia immunofluorescence. F. Number of osteoblasts per bone perimeter (N.Ob/B.Pm). G. Serum was isolated from whole blood (n = 4 mice/group); ELISA analysis of P1NP levels. Data are expressed as mean ± SEM, $^{*}p < 0.05$, $^{**}p < 0.01$, $^{***}p < 0.001$.

pubertal growing skeleton. Prior research in C5aR1$^{-/-}$ mice supports that C5aR1 signaling negatively affects skeletal bone mass (Kovtun et al., 2017). However, the role that C3aR signaling plays in skeletal modeling and bone mass is currently unclear. Therefore, to discern C3aR signaling effects on post pubertal skeletal growth, micro-CT analysis was conducted in the femur of C3aR$^{-/-}$ vs. wildtype mice to evaluate differences in trabecular (Fig. 4A-G) and cortical (Fig. 4H-K) bone morphology and mineral density. Paralleling the enhanced skeletal phenotype found in C3aR$^{-/-}$C5aR$^{-/-}$ vs. wildtype mice, there was a 22.6 % increase in trabecular bone volume fraction in C3aR$^{-/-}$ vs. wildtype mice (Fig. 4C). The increased bone volume fraction in C3aR$^{-/-}$ mice was accredited to higher connectivity density (Fig. 4D) and increased trabecular number (Fig. 4E), while there were no alterations in trabecular thickness (Fig. 4F) or trabecular separation (Fig. 4G). Cortical bone mineral density (Fig. 4I), cortical area fraction (Fig. 4J), and cortical thickness (Fig. 4K) were similar in the femoral midiaphysis of C3aR$^{-/-}$ vs. wildtype mice. These findings support that C3aR signaling has effects on trabecular, but not cortical bone, in the young female skeleton.

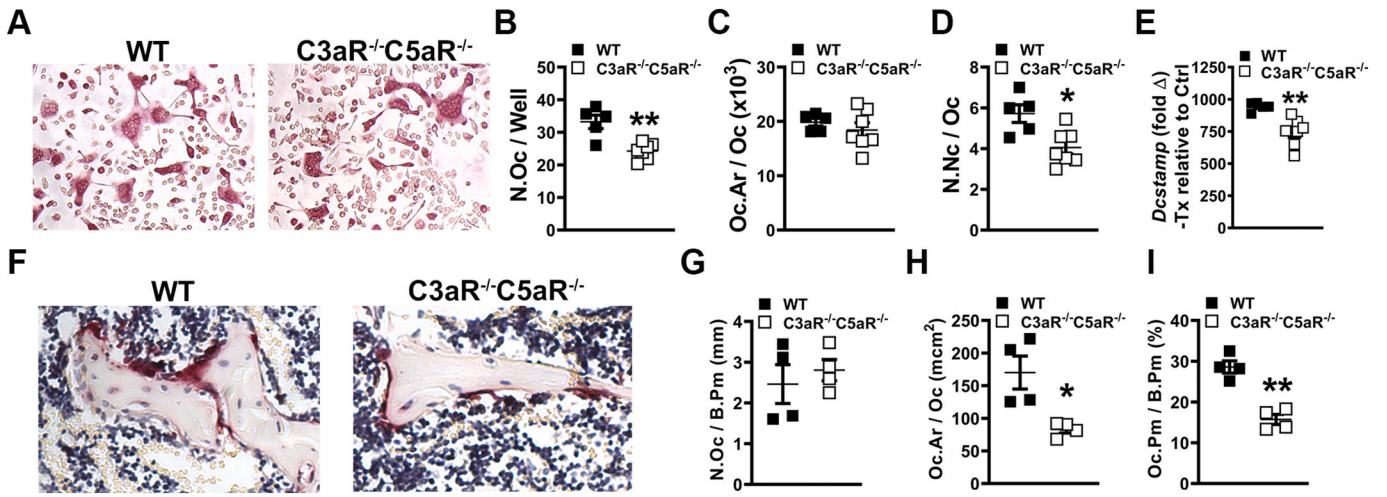

Fig. 3. Suppressed osteoclastogenesis in C3aR$^{-/-}$C5aR$^{-/-}$ vs. wildtype mice. (A-E) Wildtype (WT) and C3aR$^{-/-}$C5aR$^{-/-}$ mice were euthanized, and whole marrow cells were isolated and sorted for CD11b^{-} cells. CD11b^{-} cells were treated with CSF1 alone or CSF1 + RANKL for 5 days (n = 5–7 mice/group). A. Representative images of TRAP-stained cultures. B. Number of osteoclasts (N.Oc/Well) in day 5 cultures. C. Osteoclast size (Oc.Ar/Oc). D. Number of nuclei per osteoclast (N.Nc/Oc). E. qRT-PCR gene expression studies were conducted in CD11b^{neg} OCP cultures on day 4 to detect *Dcstamp* mRNA transcription level alterations in RANKL-stimulated osteoclast differentiation. Relative quantification of mRNA was performed via $2^{-\Delta\Delta CT}$; data expressed as treatment (CSF1 and RANKL) fold change relative to control (CSF1). (F-I) WT and C3aR$^{-/-}$C5aR$^{-/-}$ mice were euthanized, and tibiae were processed for paraffin-embedded TRAP+ staining for osteoclasts in vivo (n = 4 mice/group). F. Representative images of TRAP-stained proximal tibia histology. G. Number of osteoclasts per bone perimeter (N.Oc/B.Pm). H. Osteoclast size (Oc.Ar/Oc). I. Osteoclast perimeter per bone perimeter (Oc.Pm/B.Pm). Data are expressed as mean ± SEM, *$p < 0.05$, **$p < 0.01$.

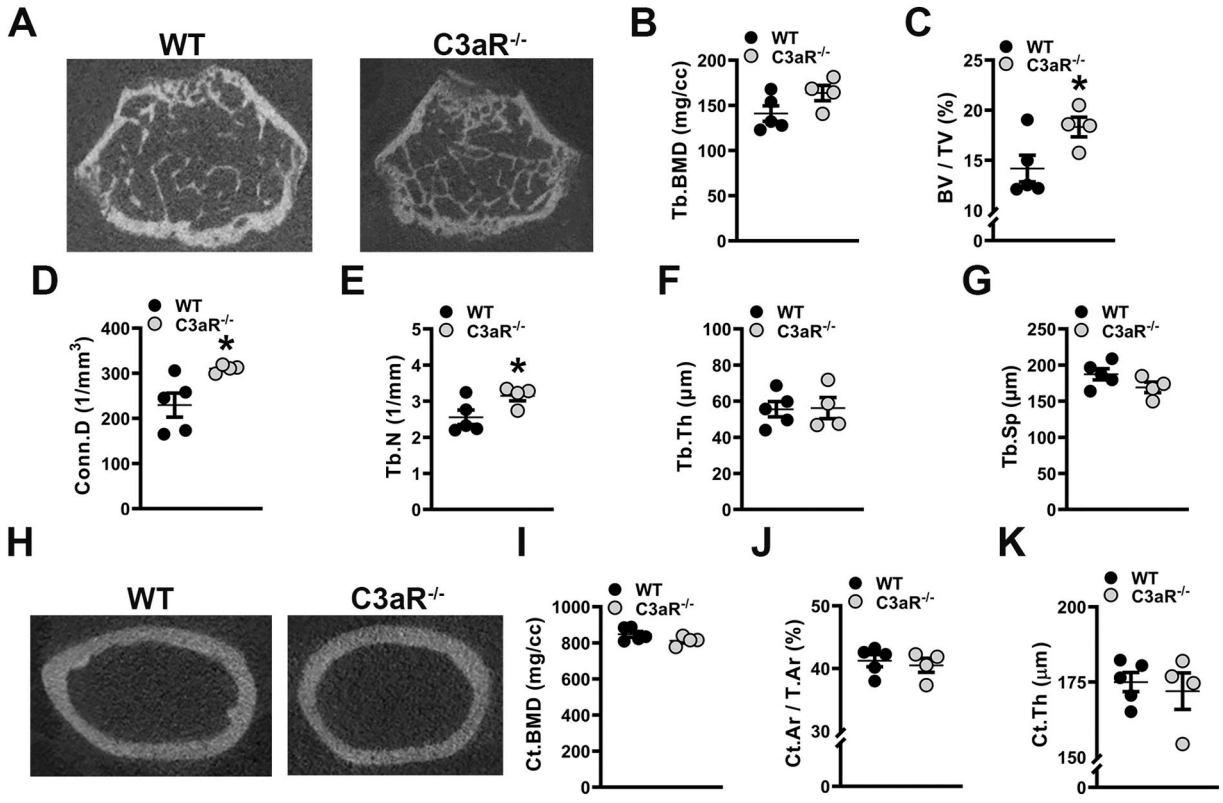

Fig. 4. C3aR$^{-/-}$ vs. wildtype mice have a superior trabecular bone phenotype. Wildtype (WT) and C3aR$^{-/-}$ mice were euthanized, and femurs were analyzed. (A-G) WT vs. C3aR$^{-/-}$ micro-CT trabecular analysis, (n = 4–5 mice/group). A. Representative micro-CT images of trabecular bone at the distal femur. B. Trabecular (Tb) bone mineral density (BMD). C. Trabecular bone volume fraction (BV/TV). D. Connectivity density (Conn.D). E. Trabecular number (Tb.N). F. Trabecular thickness (Tb.Th). G. Trabecular Separation (Tb.Sp). (H-K) WT vs. C3aR$^{-/-}$ micro-CT cortical analysis, (n = 4–5 mice/group). H. Representative micro-CT images of femur mid-diaphysis. I. Cortical BMD. J. Cortical bone area fraction (Ct.Ar/T.Ar). K. Cortical thickness (Ct.Th). Data are expressed as mean ± SEM, *$p < 0.05$, **p < 0.01.

3.5. Enhanced osteoblastogenesis in C3aR$^{-/-}$ vs. wildtype mice

Like the C3aR$^{-/-}$C5aR$^{-/-}$ cultures (Fig. 2), in vitro experiments were executed in cells derived from C3aR$^{-/-}$ vs. wildtype mice to elucidate the role of C3aR on osteoblastogenesis (Fig. 5). BMSCs derived from C3aR$^{-/-}$ vs. wildtype cultures expanded at a greater rate over time

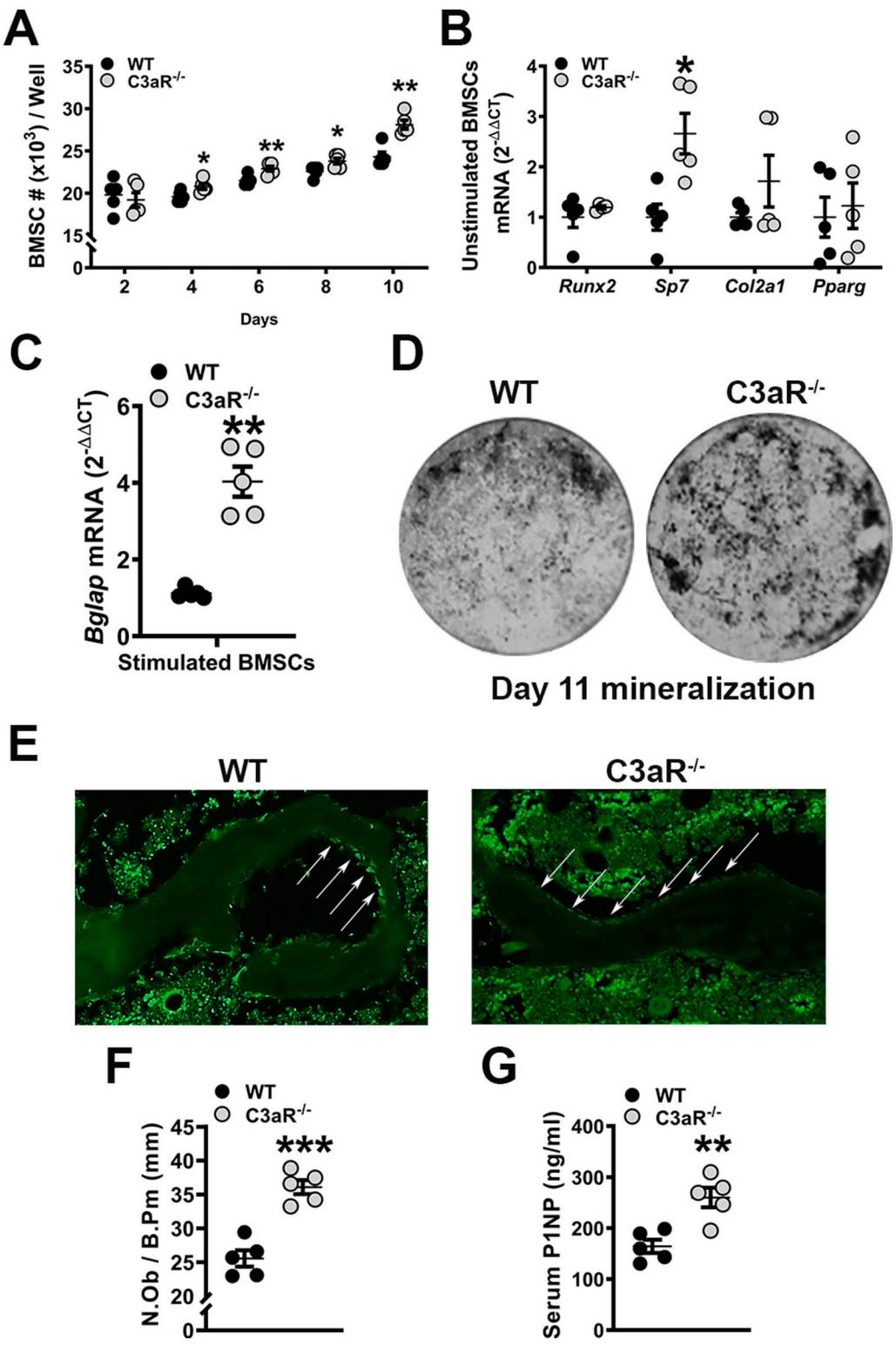

Fig. 5. Enhanced osteoblastogenesis in C3aR$^{-/-}$ vs. wildtype animals. (A–D) Wildtype (WT) and C3aR$^{-/-}$ mice were euthanized, bone marrow harvested, and BMSCs were isolated for in vitro assays. A. BMSC expansion over time in culture. B. BMSC differentiation potential assay; BMSCs were cultured for 4 days and harvested pre-confluent for qRT-PCR analysis. mRNA markers for osteoblastic (*Runx2*, *Sp7*), chondrogenic (*Col2a1*), and adipogenic (*Pparg*) potential were evaluated, and relative quantification of mRNA was performed via the comparative *C*T method ($2^{-\Delta\Delta CT}$). C. BMSC osteogenic potential assay: BMSCs stimulated with osteogenic media for 5 days were isolated for qRT-PCR analysis of *Bglap (Ocn)* mRNA. D. Representative images of day 11 mineralization cultures stained by the von Kossa method. Cultures (n = 5 mice/group) were carried out in duplicate. (E-F) WT and C3aR$^{-/-}$ mice were euthanized, and tibiae were processed for paraffin-embedded in situ immunofluorescent staining for osterix (OSX+) bone-lining osteoblasts (n = 5 mice/group). E. Representative images of OSX-stained proximal tibia immunofluorescence. F. Number of osteoblasts per bone perimeter (N.Ob/B.Pm). G. Serum was isolated from whole blood (n = 5 mice/group); ELISA analysis of P1NP levels. Data are expressed as mean ± SEM, *p < 0.05, **p < 0.01, ***p < 0.001.

(Fig. 5A). Pre-confluent untreated day-4 BMSC cultures displayed minimal changes in the commitment to the adipogenic (*Pparg*) or chondrogenic (*Col2a1*) lineages (Fig. 5B). However, C3aR$^{-/-}$ vs. wildtype cultures demonstrated a 2.5× increase in *Sp7* expression (Fig. 5B), while only a 1.5× increase was observed in C3aR$^{-/-}$C5aR$^{-/-}$ vs. wildtype cultures (Fig. 5B). Importantly, BMSCs stimulated with ascorbic acid for 5 days displayed an upregulation of *Bglap (Ocn)* in C3aR$^{-/-}$ vs. wildtype cultures (Fig. 5C). Von Kossa assays showed elevated mineralization in BMSC cultures from C3aR$^{-/-}$ vs. WT mice (Fig. 5D).

To support in vitro findings from wildtype vs. C3aR$^{-/-}$ cultures, in situ immunofluorescent staining and histomorphometric analysis of proximal tibia sections examined OSX+ bone-lining osteoblasts (Fig. 5E-F). The frequency of OSX+ osteoblasts was elevated in C3aR$^{-/-}$ vs. wildtype mice (Fig. 5F), and serum P1NP levels were enhanced in C3aR$^{-/-}$ vs. wildtype mice (Fig. 5G). These data further validate that C3aR signaling suppresses osteoblast differentiation and function.

3.6. C3aR$^{-/-}$ vs. wildtype mice have decreased osteoclast maturation

Paralleling the C3aR$^{-/-}$C5aR$^{-/-}$ vs. wildtype CD11b^{-} OCP culture outcomes at day-5, cytomorphometric analysis of TRAP-stained day-5 CD11b^{-} OCP cultures from C3aR$^{-/-}$ vs. wildtype mice (Fig. 6A-D) displayed decreased number of osteoclasts (Fig. 6B) and osteoclast area (Fig. 6C) in cultures from C3aR$^{-/-}$C5aR$^{-/-}$ vs. wildtype mice. These data support that C3aR expression promotes osteoclastogenesis. Treatment vs. control analysis was achieved in RANKL+CSF1 treatment cultures relative to CSF1 control cultures to evaluate *Dcstamp*. RANKL treatment enhanced *Dcstamp* in CD11b^{-} OCP cultures from wild-type vs. C3aR$^{-/-}$ mice (Fig. 6E). This data supports the notion that the C3aR immunostimulation stimulates RANKL-induced osteoclast fusion.

To determine if osteoclastogenesis is suppressed with the deletion of C3aR in vivo, histomorphometric analysis of TRAP-stained proximal tibia sections was performed in animals (Fig. 6F-I). There was a lower number of osteoclasts lining the trabecular bone perimeter (N.Oc/B.Pm) in C3aR$^{-/-}$ vs. wildtype mice (Fig. 6G), which suggests that C3aR limits the commitment of monocyte/myeloid cells to the osteoclast lineage. Osteoclast size (Oc.Ar/Oc) was not different (Fig. 6H), but osteoclast perimeter per bone perimeter (Oc.Pm/B.Pm) was reduced in C3aR$^{-/-}$ vs. wildtype mice (Fig. 6I), which indicates that C3aR promotes osteoclast maturation. The lower N.Oc/B.Pm (Fig. 6G) and Oc.Pm/B.Pm (Fig. 6I) findings in the proximal tibia align with the superior trabecular bone phenotype found in C3aR$^{-/-}$ vs. wildtype mice (Fig. 4).

3.7. Exogenous C3a induces C3ar1 and osteoclastic genes Cxcl1 and Ccl2 in osteoblasts in vitro

To elucidate the molecular underpinnings of C3a/C3aR signaling actions on osteoblasts, qRT-PCR gene expression studies were performed in osteoblast cell lysates (Fig. 7A-B), and ELISA protein analysis was carried out with osteoblast culture supernatants (Fig. 7C). Gene expression studies were performed in wildtype osteoblasts with varying concentrations of C3a to evaluate alterations in *C3ar1* mRNA. *C3ar1* was significantly increased in osteoblasts treated with C3a at a concentration of 20 ng/mL (Fig. 7A). Interestingly, there was a trending increase in *Ccl2* and a significant upregulation in *Cxcl1* observed in osteoblasts stimulated with exogenous C3a (Fig. 7B). CCL2 and CXCL1 were examined as osteoblast-derived CCL2 paracrine signaling has been shown to support osteoclast fusion/maturation (Hathaway-Schrader et al., 2022; Li et al., 2007b; Khan et al., 2016). ELISA C3a analysis of cell supernatants from stimulated osteoblasts revealed no differences in C3a protein (Fig. 7C), suggesting that circulating C3a protein is not osteoblast-derived. These data suggest that C3a signaling induces osteoblast-derived signaling factors to support osteoclastogenesis.

4. Discussion

The complement system, a critical component of innate immunity, has been evaluated in various aspects of the musculoskeletal field. Complement involvement in bone has included homeostasis (Ignatius et al., 2011; Ehrnthaller et al., 2011; Andrades et al., 1996), regeneration (Ehrnthaller et al., 2016), inflammation (Ignatius et al., 2011; Banda et al., 2012; Murayama et al., 2015), alveolar bone (Hajishengallis et al., 2011; Liang et al., 2011), and more. Though the anaphylatoxin receptor C5aR has been primarily described in bone fracture and repair (Ignatius et al., 2011; Kovtun et al., 2017; Ehrnthaller et al., 2016; Bergdolt et al., 2017), C3a/C3aR signaling and expression have not been as well-characterized in health and pathological skeletal conditions.

The present study describes the loss of C3aR leads to a higher trabecular bone phenotype in young, growing mice. Interestingly, bone volume fraction was increased by 22.6 % in C3aR$^{-/-}$ vs. wildtype. Additionally, C3aR$^{-/-}$ vs. wildtype cultures demonstrated a 2.5× increase in *Sp7* expression. Corroborating the *Sp7* expression in unstimulated BMSCs, there was a 4-fold difference in *Bglap (Ocn)* expression in C3aR$^{-/-}$ vs. wildtype stimulated cultures. Interestingly, C3aR$^{-/-}$ vs. wildtype mice had profound differences in osteoblast numbers and serum P1NP in vivo. This implies that C3aR alone may regulate skeletal homeostasis and osteoblast differentiation. On the other hand, the knockdown of C3aR/C5aR and C3aR alone similarly suppressed osteoclastic genes and numbers in vitro, validating findings from Tu et al. (Tu et al., 2010) While the current studies were performed in global knockout murine models, future investigations are crucial to determine whether bone cell-specific knockouts of C3aR may alter skeletal growth in health and disease.

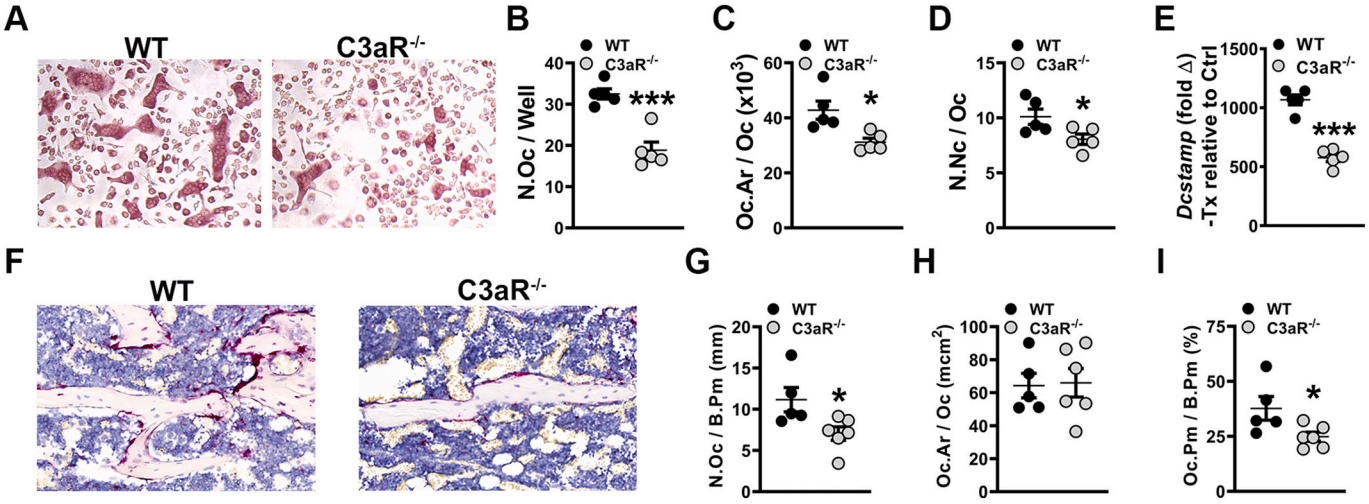

Fig. 6. C3aR$^{-/-}$ vs. wildtype mice show a decreased osteoclast phenotype. (A-E) Wildtype (WT) and C3aR$^{-/-}$ mice were euthanized, and whole marrow cells were isolated and sorted for CD11b^{-} cells. CD11b^{-} cells were treated with CSF1 alone or CSF1 + RANKL for 5 days (n = 5 mice/group). A. Representative images of TRAP-stained cultures. B. Number of osteoclasts per well (N.Oc/Well) in day 5 cultures. C. Osteoclast size in day 5 cultures (Oc.Ar/Oc). D. Number of nuclei per osteoclast (N.Nc/Oc) in day 5 cultures. E. qRT-PCR gene expression studies were conducted in CD11b^{neg} OCP cultures on day 4 to detect *Dcstamp* mRNA transcription level alterations in RANKL-stimulated osteoclast differentiation. Relative quantification of mRNA was performed via $2^{-\Delta\Delta CT}$; data expressed as treatment (CSF1 and RANKL) fold change relative to control (CSF1). (F-I) WT and C3aR$^{-/-}$ mice were euthanized, and tibiae were processed for paraffin-embedded TRAP+ staining for osteoclasts in vivo ($n = 4$ mice/group). F. Representative images of TRAP-stained proximal tibia histology. G. Number of osteoclasts per bone perimeter (N.Oc/B.Pm). H. Osteoclast size (Oc.Ar/Oc). I. Osteoclast perimeter per bone perimeter (Oc.Pm/B.Pm). Data are expressed as mean ± SEM. *p < 0.05, ***p < 0.001.

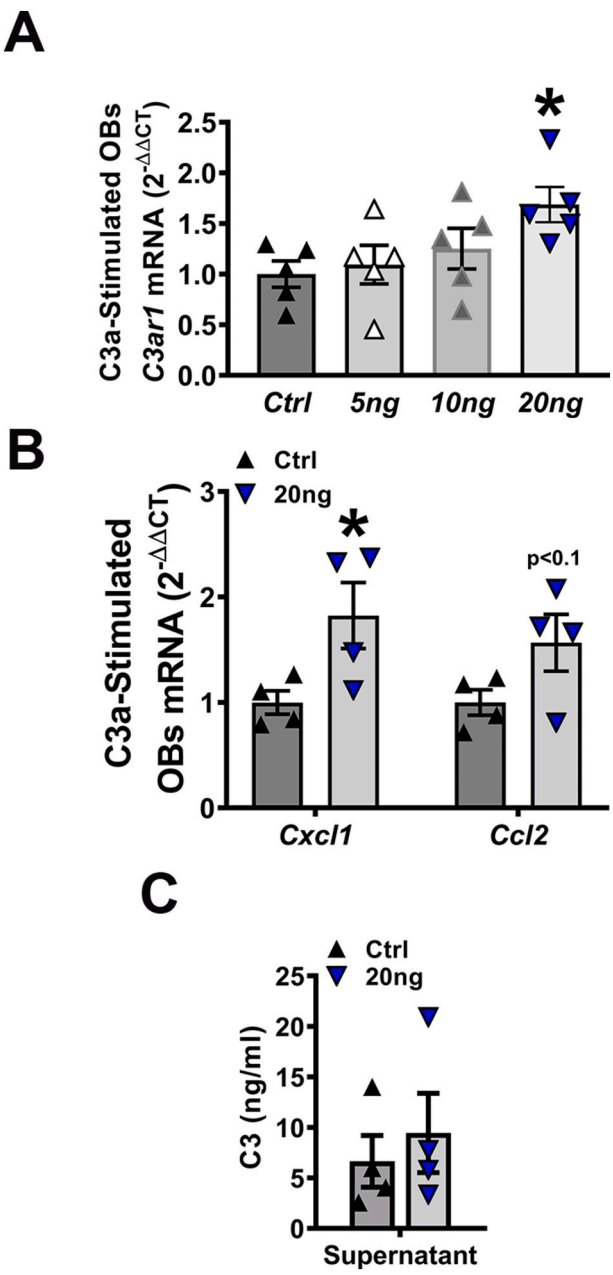

Fig. 7. Exogenous C3a induces *C3ar1* and osteoclastic genes *Cxcl1* and *Ccl2* in osteoblasts in vitro. Wildtype bone marrow stromal cells treated with osteogenic media were stimulated with or without C3a for 2 h; cells & supernatants were collected for qRT-PCR and ELISA analyses. A. qRT-PCR analysis of *C3ar1* mRNA in osteoblasts stimulated with varying concentrations (0-20 ng) of C3a; n = 4 mice/group. B. qRT-PCR analysis of *Cxcl1* and *Ccl2* mRNA in osteoblasts stimulated with Ctrl or 20 ng C3a; n = 4 mice/group. mRNA quantification of data via the $2^{-\Delta\Delta CT}$ method. C. ELISA analysis of C3a in cell supernatants derived from osteoblasts stimulated with Ctrl or 20 ng C3a; n = 4 mice/group. Data are expressed as mean ± SEM. $^{*}p < 0.05$.

The current report highlights the role of C3a/C3aR signaling in the growing skeleton; yet it is important to note skeletal alterations observed in $C3aR^{-/-}C5aR^{-/-}$ vs. wildtype mice. Although peak trabecular and cortical bone mass is not achieved simultaneously, there was a significant elevation of both trabecular and cortical bone mineral densities in $C3aR^{-/-}C5aR^{-/-}$ vs. wildtype mice. Knockouts of other complement subunits (i.e., C3, C5, CD59) have been shown to alter skeletal structure and architecture, such as blunted endochondral ossification, thicker epiphyseal growth plates, and increased cortical bone area (Ehrnthaller et al., 2013; Bloom et al., 2016). Considering there were no differences in cortical bone outcomes or bone mineral density in $C3aR^{-/-}$ vs. wildtype mice, our findings suggest a distinct role of C5aR, with or without C3aR synergistic effects, promoting peak bone mineral density. Further experimentation is needed to define the specific functions of C3aR and C5aR in cortical bone development and bone mineral density achievement.

C3 can be secreted by various cell types deriving from the mesenchymal and hematopoietic stem cell lineages (Ricklin et al., 2010; Reis et al., 2019). Osteoblasts can secrete C3 and C5, while osteoclasts can only secrete C3 (Ignatius et al., 2011). Therefore, the source of C3a signaling to C3aR on bone cells remains unclear. Previous reports have shown that C3 produced by osteoblasts can impact osteoclasts (Ignatius et al., 2011), but osteoclast-derived C3a can also promote osteoblast differentiation (Matsuoka et al., 2014). However, the bone marrow microenvironment includes numerous cells expressing and secreting C3. Defining the source of C3a to signal at C3aR on various bone cells would advance knowledge about osteoimmunological mechanisms between osteoblasts, osteoclasts, and their precursors.

Limitations of the current study involve evaluating skeletal outcomes at one time point. While trabecular and cortical bone modeling/remodeling are vastly different and are achieved at various times, it is important to elucidate the role of C3aR in the adult/aging skeleton. Another limitation of the present report includes possible sex differences, where alterations in skeletal outcomes with CD59 may be gender specific (Bloom et al., 2016). However, Kovtun et al. (2017) reported that both $C5aR1^{-/-}$ and $C5aR2^{-/-}$ male mice displayed elevated bone mass, with increases in osteoblast numbers and decreases in osteoclast formation (Kovtun et al., 2017). Although C3aR was not evaluated in Kovtun et al. (2017), future experimentation would be needed to determine whether C3aR and C5aR are sex-dependent for skeletal outcomes. Further drawbacks include elucidating the contribution of osteoblasts vs. osteoclasts towards the observed skeletal phenotype, where co-culture experimentation of osteoblasts and osteoclasts would be ideal. However, by the time primary BMSC/osteoblast cultures are properly differentiated, OCPs derived from the same animals are short-lived, having reached full osteoclastic potential, and cannot be expanded. While studies are trying to improve co-culture models in 3D (Remmers et al., 2023), previous reports have utilized cell lines, such as RAW267.4 cells treated with RANKL, to examine osteoblast-derived factors on osteoclastogenesis (Hathaway-Schrader et al., 2022). The RAW264.7 cell line can be employed as a control, as opposed to pre-existing changes in OCPs derived from wildtype and knockout mice. Further experimentation is necessary to clarify the role of C3aR on osteoblast and osteoclast activities during skeletal growth.

The late pubertal/young adult phase accounts for approximately 40 % of peak bone accrual (Weaver et al., 2016; Bonjour et al., 1991; Cheung et al., 2011; McCormack et al., 2017). Understanding osteoimmunological processes, such as C3a/C3aR signaling, during this critical growth period will afford opportunities to optimize bone mass accrual. Notably, knowledge about interventions, such as targeted bone-derived C3aR or C3aR/C5aR inhibitors, optimizing skeletal growth may have life-long implications for skeletal health and fracture risk. Future studies are needed for targeting C3a/C3aR both in the growing skeleton and preventing skeletal deterioration in pathophysiological states.

5. Conclusions

This study suggests that the C3aR signaling axis may critically regulate osteoblast-osteoclast-mediated bone modeling/remodeling processes in skeletal homeostasis.

CRediT authorship contribution statement

JDH and CMN conceived the study design. MBK, HSV, AJR, MDC, AJW, ACL, CMN and JDH performed data acquisition and analysis. ACL,

CMN and JDH interpreted the data. JDH drafted the manuscript. All authors approved the final version of the manuscript. JDH takes responsibility for the integrity of the data analysis.

Funding sources

IK2BX005813-01A1, NIH/NIDCR K08DE025337, American Society for Bone and Mineral Research Rising Star Award, SCTR Voucher 12477-0001, NIH/NIDCR R01DE029637, NIH/NIGMS P20GM13045, NIH/NIGMS P20GM121342, NIH/NIDCR T32DE017551, NIH/NIDDK P30DK123704.

Declaration of competing interest

All authors, Megan B. Kuhn, Hayden S. Vandenburg, Andrew J. Reynolds, Matthew D. Carson, Amy J. Warner, Amanda C. LaRue, Chad M. Novince, and Jessica D. Hathaway-Schrader, declare no conflicts of interest.

Data availability

Data will be made available on request.

Acknowledgments

The authors thank Dr. Carl Atkinson for the C3aR$^{-/-}$C5aR$^{-/-}$ and the C3aR$^{-/-}$ mice.

References

Andrades, J.A., Nimni, M.E., Becerra, J., Eisenstein, R., Davis, M., Sorgente, N., 1996. Complement proteins are present in developing endochondral bone and may mediate cartilage cell death and vascularization. Exp. Cell Res. 227 (2), 208–213.
Banda, N.K., Hyatt, S., Antonioli, A.H., et al., 2012. Role of C3a receptors, C5a receptors, and complement protein C6 deficiency in collagen antibody-induced arthritis in mice. J. Immunol. 188 (3), 1469–1478.
Baxter-Jones, A.D., Faulkner, R.A., Forwood, M.R., Mirwald, R.L., Bailey, D.A., 2011. Bone mineral accrual from 8 to 30 years of age: an estimation of peak bone mass. J. Bone Miner. Res. 26 (8), 1729–1739.
Bergdolt, S., Kovtun, A., Hagele, Y., et al., 2017. Osteoblast-specific overexpression of complement receptor C5aR1 impairs fracture healing. PLoS One 12 (6), e0179512.
Bloom, A.C., Collins, F.L., Van't Hof, R.J., et al., 2016. Deletion of the membrane complement inhibitor CD59a drives age and gender-dependent alterations to bone phenotype in mice. Bone 84, 253–261.
Bonjour, J.P., Theintz, G., Buchs, B., Slosman, D., Rizzoli, R., 1991. Critical years and stages of puberty for spinal and femoral bone mass accumulation during adolescence. J. Clin. Endocrinol. Metab. 73 (3), 555–563.
Bouxsein, M.L., Boyd, S.K., Christiansen, B.A., Guldberg, R.E., Jepsen, K.J., Muller, R., 2010. Guidelines for assessment of bone microstructure in rodents using micro-computed tomography. J. Bone Miner. Res. 25 (7), 1468–1486.
Cheung, W.W., Zhan, J.Y., Paik, K.H., Mak, R.H., 2011. The impact of inflammation on bone mass in children. Pediatr. Nephrol. 26 (11), 1937–1946.
Dempster, D.W., Compston, J.E., Drezner, M.K., et al., 2013. Standardized nomenclature, symbols, and units for bone histomorphometry: a 2012 update of the report of the ASBMR histomorphometry nomenclature committee. J. Bone Miner. Res. 28 (1), 2–17.
Ehrnthaller, C., Ignatius, A., Gebhard, F., Huber-Lang, M., 2011. New insights of an old defense system: structure, function, and clinical relevance of the complement system. Mol. Med. 17 (3–4), 317–329.
Ehrnthaller, C., Huber-Lang, M., Nilsson, P., et al., 2013. Complement C3 and C5 deficiency affects fracture healing. PLoS One 8 (11), e81341.
Ehrnthaller, C., Huber-Lang, M., Kovtun, A., et al., 2016. C5aR inhibition in the early inflammatory phase does not affect bone regeneration in a model of uneventful fracture healing. Eur. J. Med. Res. 21 (1), 42.
Ferguson, V.L., Ayers, R.A., Bateman, T.A., Simske, S.J., 2003. Bone development and age-related bone loss in male C57BL/6J mice. Bone 33 (3), 387–398.
Glatt, V., Canalis, E., Stadmeyer, L., Bouxsein, M.L., 2007. Age-related changes in trabecular architecture differ in female and male C57BL/6J mice. J. Bone Miner. Res. 22 (8), 1197–1207.
Hajishengallis, G., Lambris, J.D., 2016. More than complementing tolls: complement-toll-like receptor synergy and crosstalk in innate immunity and inflammation. Immunol. Rev. 274 (1), 233–244.
Hajishengallis, G., Liang, S., Payne, M.A., et al., 2011. Low-abundance biofilm species orchestrates inflammatory periodontal disease through the commensal microbiota and complement. Cell Host Microbe 10 (5), 497–506.
Hathaway-Schrader, J.D., Steinkamp, H.M., Chavez, M.B., et al., 2019. Antibiotic perturbation of gut microbiota dysregulates osteoimmune cross talk in postpubertal skeletal development. Am. J. Pathol. 189 (2), 370–390.
Hathaway-Schrader, J.D., Poulides, N.A., Carson, M.D., et al., 2020. Specific commensal bacterium critically regulates gut microbiota osteoimmunomodulatory actions during Normal postpubertal skeletal growth and maturation. JBMR Plus. 4 (3), e10338.
Hathaway-Schrader, J.D., Carson, M.D., Gerasco, J.E., et al., 2022. Commensal gut bacterium critically regulates alveolar bone homeostasis. Lab. Investig. 102 (4), 363–375.
Ignatius, A., Schoengraf, P., Kreja, L., et al., 2011. Complement C3a and C5a modulate osteoclast formation and inflammatory response of osteoblasts in synergism with IL-1beta. J. Cell. Biochem. 112 (9), 2594–2605.
Jacquin, C., Gran, D.E., Lee, S.K., Lorenzo, J.A., Aguila, H.L., 2006. Identification of multiple osteoclast precursor populations in murine bone marrow. J. Bone Miner. Res. 21 (1), 67–77.
Khan, U.A., Hashimi, S.M., Bakr, M.M., Forwood, M.R., Morrison, N.A., 2016. CCL2 and CCR2 are essential for the formation of osteoclasts and foreign body Giant cells. J. Cell. Biochem. 117 (2), 382–389.
Kovtun, A., Bergdolt, S., Hagele, Y., et al., 2017. Complement receptors C5aR1 and C5aR2 act differentially during the early immune response after bone fracture but are similarly involved in bone repair. Sci. Rep. 7 (1), 14061.
Landreth, K.S., 2002. Critical windows in development of the rodent immune system. Hum. Exp. Toxicol. 21 (9–10), 493–498.
Li, Y., Toraldo, G., Li, A., et al., 2007. B cells and T cells are critical for the preservation of bone homeostasis and attainment of peak bone mass in vivo. Blood 109 (9), 3839–3848.
Li, X., Qin, L., Bergenstock, M., Bevelock, L.M., Novack, D.V., Partridge, N.C., 2007. Parathyroid hormone stimulates osteoblastic expression of MCP-1 to recruit and increase the fusion of pre/osteoclasts. J. Biol. Chem. 282 (45), 33098–33106.
Liang, S., Krauss, J.L., Domon, H., et al., 2011. The C5a receptor impairs IL-12-dependent clearance of porphyromonas gingivalis and is required for induction of periodontal bone loss. J. Immunol. 186 (2), 869–877.
Lorenzo, J., Horowitz, M., Choi, Y., 2008. Osteoimmunology: interactions of the bone and immune system. Endocr. Rev. 29 (4), 403–440.
Matsuoka, K., Park, K.A., Ito, M., Ikeda, K., Takeshita, S., 2014. Osteoclast-derived complement component 3a stimulates osteoblast differentiation. J. Bone Miner. Res. 29 (7), 1522–1530.
McCormack, S.E., Cousminer, D.L., Chesi, A., et al., 2017. Association between linear growth and bone accrual in a diverse cohort of children and adolescents. JAMA Pediatr. 171 (9), e171769.
Modinger, Y., Rapp, A., Pazmandi, J., et al., 2018. C5aR1 interacts with TLR2 in osteoblasts and stimulates the osteoclast-inducing chemokine CXCL10. J. Cell. Mol. Med. 22 (12), 6002–6014.
Murayama, M.A., Kakuta, S., Inoue, A., et al., 2015. CTRP6 is an endogenous complement regulator that can effectively treat induced arthritis. Nat. Commun. 6, 8483.
Novince, C.M., Whittow, C.R., Aartun, J.D., et al., 2017. Commensal gut microbiota immunomodulatory actions in bone marrow and liver have catabolic effects on skeletal homeostasis in health. Sci. Rep. 7 (1), 5747.
Pobanz, J.M., Reinhardt, R.A., Koka, S., Sanderson, S.D., 2000. C5a modulation of interleukin-1 beta-induced interleukin-6 production by human osteoblast-like cells. J. Periodontal Res. 35 (3), 137–145.
Recknagel, S., Bindl, R., Kurz, J., et al., 2012. C5aR-antagonist significantly reduces the deleterious effect of a blunt chest trauma on fracture healing. J. Orthop. Res. 30 (4), 581–586.
Redlich, K., Smolen, J.S., 2012. Inflammatory bone loss: pathogenesis and therapeutic intervention. Nat. Rev. Drug Discov. 11 (3), 234–250.
Reis, E.S., Mastellos, D.C., Hajishengallis, G., Lambris, J.D., 2019. New insights into the immune functions of complement. Nat. Rev. Immunol. 19 (8), 503–516.
Remmers, S.J.A., van der Heijden, F.C., de Wildt, B.W.M., Ito, K., Hofmann, S., 2023. Tuning the resorption-formation balance in an in vitro 3D osteoblast-osteoclast co-culture model of bone. Bone Rep. 18, 101646.
Ricklin, D., Hajishengallis, G., Yang, K., Lambris, J.D., 2010. Complement: a key system for immune surveillance and homeostasis. Nat. Immunol. 11 (9), 785–797.
Sato, T., Abe, E., Jin, C.H., et al., 1993. The biological roles of the third component of complement in osteoclast formation. Endocrinology 133 (1), 397–404.
Schmittgen, T.D., Livak, K.J., 2008. Analyzing real-time PCR data by the comparative C (T) method. Nat. Protoc. 3 (6), 1101–1108.
Takayanagi, H., 2009. Osteoimmunology and the effects of the immune system on bone. Nat. Rev. Rheumatol. 5 (12), 667–676.
Tu, Z., Bu, H., Dennis, J.E., Lin, F., 2010. Efficient osteoclast differentiation requires local complement activation. Blood 116 (22), 4456–4463.
Walsh, M.C., Takegahara, N., Kim, H., Choi, Y., 2018. Updating osteoimmunology: regulation of bone cells by innate and adaptive immunity. Nat. Rev. Rheumatol. 14 (3), 146–156.
Weaver, C.M., Gordon, C.M., Janz, K.F., et al., 2016. The National Osteoporosis Foundation's position statement on peak bone mass development and lifestyle factors: a systematic review and implementation recommendations. Osteoporos. Int. 27 (4), 1281–1386.
Weitzmann, M.N., Ofotokun, I., 2016. Physiological and pathophysiological bone turnover - role of the immune system. Nat. Rev. Endocrinol. 12 (9), 518–532.
Zaidi, M., 2007. Skeletal remodeling in health and disease. Nat. Med. 13 (7), 791–801.